Ionospheric Total Electron Content and Scintillation Variations over Uzbekistan and China GPS stations during the Annular Solar Eclipse on 21 June 2020

H.E Eshkuvatov[1,2*] and B.J Ahmedov[2,3†]

[1*]Ulugh Beg Astronomical Institute, Astronomy St.33, Tashkent, 100052, Uzbekistan.
[2]National University of Uzbekistan , University St.4, Tashkent, 1000174, Uzbekistan.
[3] Institute of Fundamental and Applied Research, National Research University TIIAME, Kori Niyoziy 39, Tashkent, 100000, Uzbekistan.

*Corresponding author(s). E-mail(s): husan@astrin.uz;
Contributing authors: ahmedov@astrin.uz;
†These authors contributed equally to this work.

Abstract

In this study, we utilized both ground-based and space-borne observations including total electron content (TEC) from GPS satellites. We investigate in detail variations of ionospheric Total Electron Content (TEC) and Ionospheric Scintillation Index S4 during the annular Solar eclipse that occurred on 21st June 2020 over selected sites. We choose six stations MTAL, KIT3, and MADK in Uzbekistan, and JFNG, LHAZ, and BJFS in China which are located close to the path of the Solar eclipse with obscuration **52%**, **57%**, **58%**, and **92%**, **94%** and **95%**, respectively. The Ionospheric parameters as TEC and S4 index have been analyzed for continuous three days from 20th to 22nd June 2020. A significant amount of depletion in TEC of the order of 10-30 **%** has been observed concerning the solar eclipse day. The results of the performed analysis indicate that the TEC level and S4 scintillation index were decreased during the solar eclipse due to the contraction of ionizing radiation.

Keywords: keyword1, Keyword2, Keyword3, Keyword4

1 Introduction

The study of the effects of Solar eclipses on the ionosphere's main parameters is one of the most important current tasks being explored extensively in the literature (See e.g. [1], [2], [3], [4]). During a Solar eclipse, the ionosphere is affected due to complete or partial obstruction of solar radiation. This leads to a decrease in the number of electrons and ions in the F- a layer of the ionosphere. Several factors contribute to the F-layer of ionosphere upheavals: the degree of solar and geomagnetic disturbances, latitude and longitude, and local time. These factors lead to a change in ionization in the F- the region of the ionosphere during a solar eclipse, where dynamic processes play an important role. Many studies have been extensively studied over the past years on the relationship between solar eclipses and total electron content variations ([20], [21], [22], [23]). The total amount of electrons is a good indicator of the state and dynamics of the F-region of the ionosphere. The dynamics of the ionosphere during a Solar eclipse can be analyzed based on TEC monitoring. The dynamic effects of the ionosphere during a solar eclipse were studied by satellite measurements ([5], [6], [7]).

As a result of changes in altitude in the neutral composition of the atmosphere and the rate of production with altitude, the plasma density in the ionosphere has vertical layer structures defined as layers D, E, F. These layers are controlled by different physical and chemical processes and have different compositions of ions. The effects of various solar flares and solar eclipses and extraterrestrial events can disrupt the physical and chemical properties of the ionosphere layers, see e.g. [8], [9], [10]. This distortion can modulate the radio signal accordingly. The D- and E- layers are also reported to be related to the sporadic metal layers [11],[12].

A solar eclipse can occur when the Moon passes between the Earth and the Sun on the new moon. If at that time the shadow of the Moon falls on the Earth's surface, part of the solar disk will be covered or "eclipsed" by the moon. At least twice a year, the geometry is flattened so that part of the moon's shadow falls on the Earth's surface and the solar eclipse is visible from that area. This study is based on GPS data-based TEC measurements ([39], [40], [41], [42]) and a study of the ionospheric effects on solar eclipses based on GPS amplitude scintillations. The shadow of the moon consists of two parts, which are a semi-shadow and an umbra and it is shown in Fig.1. The map of the visibility of the annular solar eclipse on June 21, 2020, is shown in Fig. 2.

It is also well known that the effect of a Solar eclipse is varied in terms of the location, season, atmospheric region, time of occurrence, duration, and types (partial, annular, and total) of the eclipse. This topic is becoming an attractive branch of study to the radio/ionosphere science community. In the paper [13] it has been observed that the total electron content (TEC) in F-layer derived from the ground-based Global Navigation Satellite System (GNSS) receivers experiences a significant N_e enhancement over the continental United States (CONUS) near the first contact of the total Solar eclipse occurred on 21st August 2017. The decrease in Solar radiation flux in the ionosphere during a Solar eclipse causes several observable consequences, such as a decrease in electron density in layer E and layer F1 due to plasma transport and dynamics of chemical reactions. The associated change in height in ionosphere layer boundary and the appearance and propagation of gravity waves together with several related events during the Solar eclipses have been studied e.g. in [14],[15], [16],

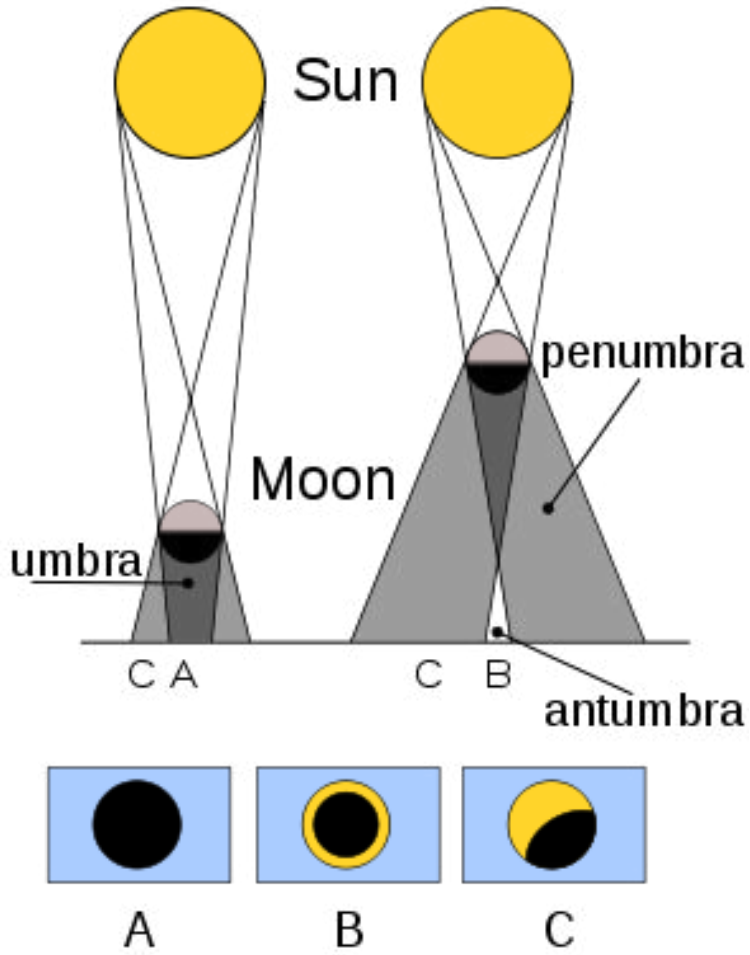

Fig. 1 Categories of Solar Eclipses: A is a total solar eclipse, B is an annular solar eclipse, and C is a partial solar eclipse. https://eclipse.gsfc.nasa.gov/.

[17], [18], [19]. The Solar eclipse provides an opportunity to study the reaction of the thermosphere and ionosphere due to the sharp decrease in the values of the ionizing radiation of the Sun produced by the partial occlusion of the solar disk by the moon. In [24] a quantitative prediction of the impact of this upcoming solar eclipse on the I–T system has been described by using Thermosphere–Ionosphere–Electrodynamics General Circulation Model simulations. A prominent total electron content (TEC) enhancement of order of 2 TEC units occurred in the equatorial ionization anomaly

Fig. 2 A globe view of the path of the annular Solar eclipse occurred on June 21, 2020. https://eclipse.gsfc.nasa.gov/.

region when this region was still in the shadow of the eclipse. The processes described above lead to the formation of plasma, which in turn chemically reacts with neutrals, disperse under the influence of gravity and pressure gradients, and is transported by neutral winds and electric fields under the influence of a magnetic field. It is found in [25] that anomalous echoes were propagated by field-aligned irregularities (FAIs) in the E-region, according to the simulated ray propagation paths of the reflected and scattered waves.

An annular solar eclipse occurs when the Moon and the Earth coincide exactly, but the Moon's visible size is smaller than that of the Sun. Thus, the Sun appears in the form of a very bright ring or ring that surrounds the dark disk of the Moon, and numerous researchers have studied the effects of solar eclipses on the ionosphere (See, e.g. [26], [27], [28], [29], [30], [31], [32], [33], [34]. [35]). Ionospheric disturbances at low latitudes can disrupt the amplitude and phase of radio signal propagation, an effect known as scintillation. Scintillations depend on various factors including the roughness strength and layer thickness, signal frequency, local time, season, solar and magnetic activity, the zenith angle of the satellite, and the angle between the radiation path and the Earth's magnetic field. Scintillation typically occurs when the Fresnel measurement of the propagating radio wave is at the level of the disordered scale in the ionosphere [36]. Maidanak and Maidantal GPS stations are installed by the regional research network Water in Central Asia (CAWa) coordinated by the German Research Centre for Geosciences (GFZ-Potsdam), Germany in cooperation with Ulugh Beg Astronomical Institute and UzHydromet, Uzbekistan. Maidanak is an internationally recognized observatory with excellent atmospheric conditions for optical astronomical observations ([37], [38]). By studying the changes in the ionosphere during a Solar eclipse, it is possible to predict the time of the solar eclipse and obtain an analysis of

Table 1 GPS stations information for TEC measurements made in this research

Station	Longitude	Latitude	Eclipse Mag(Area)
MTAL, Maidantal, Tashkent, Uzbekistan	70° 38′	41° 59′	0.6119 (52%)
KIT3, Kitab, Kashkadarya, Uzbekistan	66° 53′	39° 08′	0.6545 (57%)
MADK, Maidanak, Kashkadarya, Uzbekistan	66° 53′	38° 40′	0.6668 (58%)
JFNG, Jiufeng, Fujion, China	114° 29′	30° 30′	0.9434 (92%)
LHAZ, Lhasa, China	91° 06′	29° 39′	0.9527 (94%)
BJFS, Fangshan, China	115° 53′	39° 36′	0.9663 (95%)

the distorted data. The paper is constructed in the following way. Section 2 is devoted to data and methods of analysis performed.

The obtained results and analyses are summarized in Section 3. In Section 4, detailed explanations and discussions are given, and, finally, a summary of conclusions is provided in Section 5.

2 Data and Methods

2.1 The TEC and VTEC measurements

We have monitored total electron content in F- layer and GPS amplitude scintillations using 6 GPS receivers located in Uzbekistan and China. MADK, MTAL, KIT3 and JFNG, LHAZ, and BJFS are GPS stations that provide real-time GPS data for calculating ionosphere parameters such as TEC and S_4 index using the full temporary permission of the selected receiver. TEC of L_1 frequency (1,575 GHz) and L_2 frequency (1,228 GHz) pseudo-bands and carrier phase ([43]) along the radiation path from the receiver to the satellite. The TEC slope measured along the line of sight of a satellite signal is called slant TEC (STEC). Receiver Independent Exchange (RINEX) tracking files in GPS data Gopi Seemala [44] provides the required (.CMN) and (.STD) output files using RINEX processing software version 3.0.2. STEC is a measure of the total number of free electrons in a column of the unit cross-section along the electromagnetic wave path between a satellite and a receiver. Typically, STEC TEC_{be} and are derived from two frequency code measurements

$$STEC = \frac{1}{40.3} \times \left(\frac{L_1^2 \times L_2^2}{L_2^2 - L_1^2} \right) \times (P_1 - P_2) + TEC_{be} \ , \tag{1}$$

where P_1 (L_1) is the pseudo-range, P_2 (L_2) is the pseudo-range and TEC_{be} is used for correction of different satellite receiver pairs incorrect line error. Vertical TEC (VTEC) is derived by obtaining a projection from the slant line to the vertical line, using a thin shell model at an altitude of 350 km, following the technique given by ([45], [46], [47],[41],[42]):

$$VTEC = STEC \times \cos \left[\arcsin \left(\frac{R_e \sin z}{R_e + h_{max}} \right) \right], \tag{2}$$

where the radius of the Earth, R_e = 6,378 km, the maximum height to the pierce point, h_{max} = 350 km, and z is the angle of elevation at the ground station. For a detailed analysis of the TEC response to a Solar eclipse, we have studied the variation of the absolute TEC across the five satellite transitions. Regional TEC models were obtained using regional baseline functions to analyze the spatial distribution of TEC during a Solar eclipse. For regional modeling of TEC, we used GPS measurements collected at about 10 IGS stations using pseudo-range code and phase measurements.

2.2 Ionospheric S_4 Index scintillations

Irregularly structured ionospheric regions can lead to diffraction and propagation of trans-ionosphere radio signals. When received on an antenna, these radio signals show random transient oscillations in amplitude and phase. This is called ionosphere scintillation. Ionosphere scintillation can cause problems such as signal strength loss, phase cycle slip, loss of receiver block, etc., and deteriorate the quality of satellite navigation systems. Ionosphere scintillation is a rapid oscillation of the phase or/and amplitude of a radio frequency signal that is generated when a signal passes through the F-a layer of the ionosphere. Scintillation occurs when a straight-wave radio frequency signal crosses a region of small-scale irregularities in electron density. Ionospheric scintillation is a well-known phenomenon that has been extensively studied a lot in the past, see e.g. [48]. However, large-scale prediction or modeling remains a difficult phenomenon. Scintillation occurs as a result of small-scale oscillations of the susceptibility index of the ionospheric environment, which in turn is the result of inhomogeneities. Ionospheric disturbances can affect satellite communication and navigation by causing the radio signals. Scintillations are routinely measured using ground-based networks of receivers. For example, a discussion of ionospheric disturbance observations by Langmuir probes on Swarm satellites is published in the paper [49].

Inhomogeneities in the ionospheric medium are produced by a wide range of phenomena (e.g. plasma bubbles) and those responsible for scintillation occur mainly in the F-layer of the ionosphere at altitudes of 200 to 1000 km. However, the primary is typically located in zone F, which is 250 to 400 km. Electronic layer asymmetries such as sporadic-E and auroral E can also cause scintillation, but their effect on GPS signals in the L range is minimal and insignificant. Ionospheric scintillation is primarily an equatorial and high-latitude ionosphere phenomenon, although it can (and does) occur at lower intensities at all latitudes. The irregularities lead to small-scale fluctuations in the refractive index and subsequent differential diffraction (propagation) of the plane wave, which causes phase changes along the phase front of the signal. As the propagation of the signal continues after passing through the zone of disturbances, phase and amplitude scintillation develops through the interference of several scattered signals. The widely used S_4 and σ ionosphere scintillation indices show the amplitude and intensity of phase scintillation affecting GPS receivers. The four quantitative S_1,S_2, S_3, S_4 indices are as follows [50]:

$$S_1 = \frac{1}{\langle I \rangle} \langle |I - \langle I \rangle| \rangle = 0.42 S_4, \tag{3}$$

$$S_2 = \frac{1}{\langle I \rangle} \sqrt{\langle (I - \langle I \rangle)^2 \rangle} = 0.52 S_4, \tag{4}$$

$$S_3 = \frac{1}{\langle I^2 \rangle} \langle |I^2 - \langle I^2 \rangle| \rangle = 0.73 S_4, \tag{5}$$

$$S_4 = \frac{1}{\langle I \rangle} \sqrt{\langle I^2 \rangle - \langle I \rangle^2}\ , \tag{6}$$

where I is the signal intensity ([51]). The index S_4 is the ratio of the standard deviation of the signal strength to the average signal strength calculated over a period of time. S_4 is a dimensionless number with a theoretical upper limit of 1.0, commonly estimated over an interval of 60 seconds. There are two defined modes of amplitude scintillation: weak and strong, which roughly correspond to the type of associated scattering.

Strong scintillation is generally thought to occur when S_4 is greater than 0.6 and is associated with a strong signal propagating of signal in the ionosphere. If the level of S_4 is less than 0.3, it is unlikely to have a significant impact on the GPS signal. An Ionosphere Scintillation Monitor (ISM) is a single or dual-frequency GPS receiver specially designed to monitor the level of ionosphere scintillation in real-time. The ISM has wide-bandwidth tracking loops to maintain lock longer during intervals of strong ionospheric scintillation, and samples at a rate of 50 Hz to calculate the scintillation statistics S_4 and σ. The wide-bandwidth tracking improves tracking through strong scintillation however loss of lock on single or multiple satellites can still occur during extreme events, requiring re-acquisition of the GPS signal.

3 Results and Analyses

To study solar eclipse effects on TEC variations an approach of daily TEC variations has been used. In this approach, single-site data are used to study daily variations of TEC by comparing three consequent days around the solar eclipse day. Variations of slant TEC derived from phase measurements for the day before, during, and after the solar eclipse along satellite passes are presented in Figures 4 and 5. They show daily slant TEC variations over MTAL and LHAZ GPS stations on the 20th, 21st, and 22nd of June 2020. These time series include GPS measurements from all satellites during 24 hours. The time interval selected by black boxes indicates the time of the solar eclipse over the selected station. These figures are shown here as a representative of similar behavior of slant TEC variations on other stations' data, i.e. MADK and KIT3 data behave as MTAL shown in Figure 4, while data of JFNG and BJFS do as LHAZ shown in Figure 5.

In addition, we investigate the Solar eclipse that occurred during quiet geomagnetic conditions. The indices K_p and A_p are usually lower than 3. In this study, the values of F10.7, K_p, A_p, and Dst indices are used to check the solar and geomagnetic activities. These indices are retrieved from the NASA OMNI web https://omniweb.gsfc.nasa.gov/ and World Data Centre Kyoto http://wdc.kugi.kyoto-u.ac.jp. Furthermore, during the annular Solar eclipse on June 21, 2020, we queried geomagnetic data and analyzed some of these data to identify the relationship between geomagnetic data and the ionosphere. The K_p index is usually lower than 3 for 21 June, 2020 and the Dst index is usually greater than

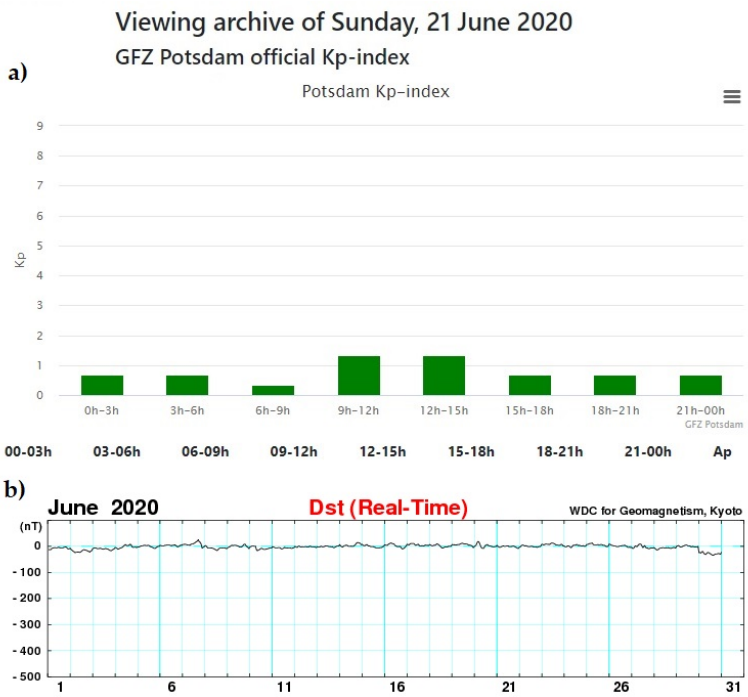

Fig. 3 Variations of (a) Kp index for 21 June 2022, (b) Dst index for the geomagnetic storms during June 2020.

-20nT are shown in Figure 3a , Figure 3b, respectively. [52] found that a thermosphere composition and ionospheric total electron content (TEC) variations during two geomagnetically quiet periods (maximum K_p=1.7) at solar minimum.

It is seen that the values of TEC during the eclipse are lower compared to the same period of other days. As it can be seen from Figure 4(b), the eclipse effect occurs as a trough-like depression. Around the maximum phase of the eclipse for each station the TEC values reach their minimum. The minimum level of TEC persists for around 20-50 minutes, and then it slowly recovers during the next 2-4 hours. The data of other stations behave analogously.

Figure 6 demonstrates vertical TEC (VTEC - slant TEC reduced to zenith) for KIT3, MTAL, LHAZ, and BJFS stations during the annular Solar eclipse. Red vertical lines denote the beginning and end of the eclipse. The behavior of TEC at the other two stations is similar to these plots. A significant decrease in the total electron content can be easily observed for all of the stations. As it can be seen, during the solar eclipse the TEC depression around 8 Universal Time (UT) is recognized for all satellites (Figure 5 - columns (b)). The time of the minimum value of TEC concerning the maximum phase of the eclipse varies in each station and the level of TEC depression is different for each satellite. A decrease in the total electron content with elevation angles was observed in several satellites at the MADK GPS station during the annular Solar eclipse, i.e., PRN 02, PRN 06, PRN 12, and PRN 25 are presented in Fig. 11 and Kitab GPS station satellites were observed, i.e. PRN 02, PRN 06, PRN 12, PRN 25

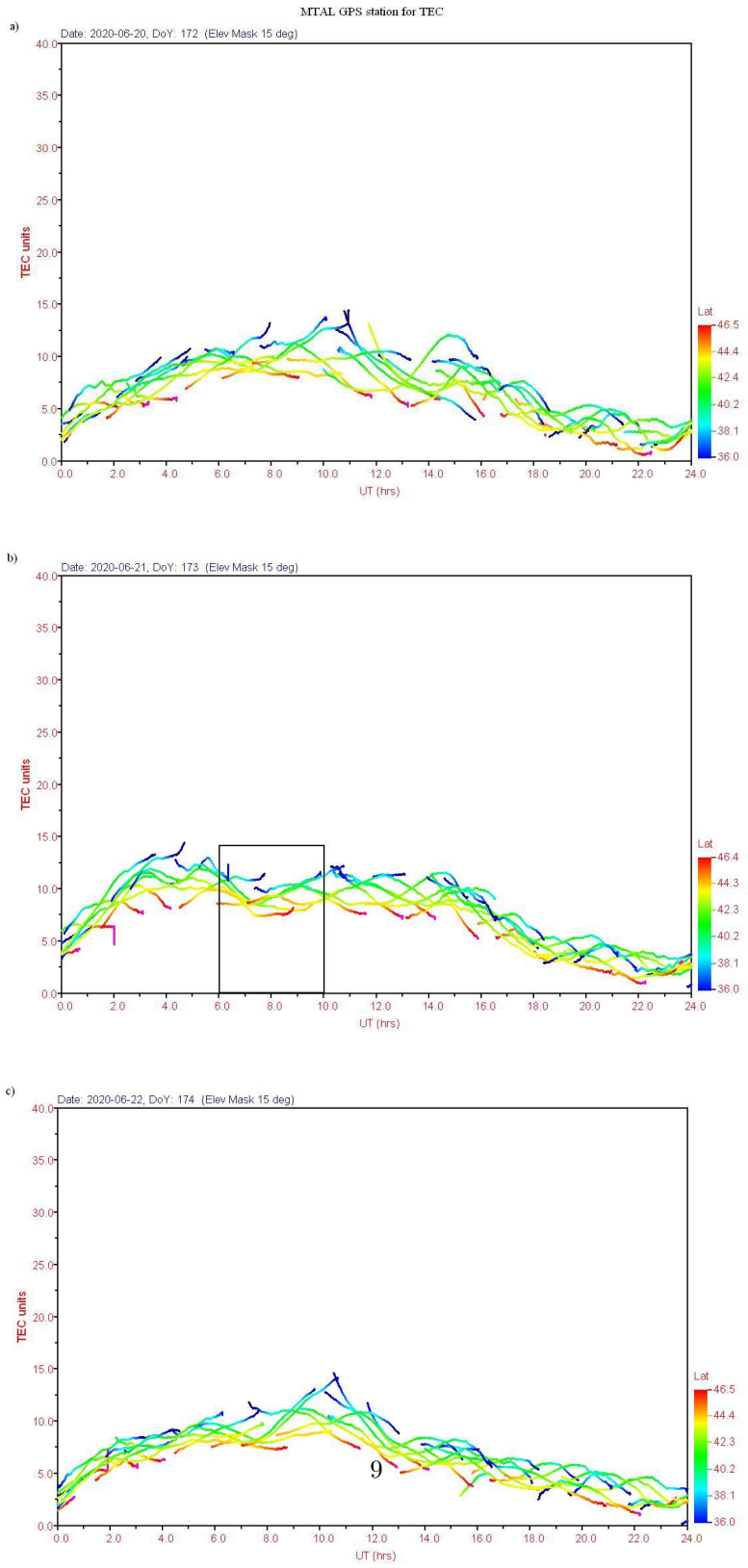

Fig. 4 Daily variation of slant TEC at MTAL GPS station on (a) 20th, (b) 21st, and (c) 22nd June 2020. The square shows the maximum phase of the solar eclipse at the MTAL GPS station in Uzbekistan. (The eclipse hours period has been indicated with the black box in column (b)).

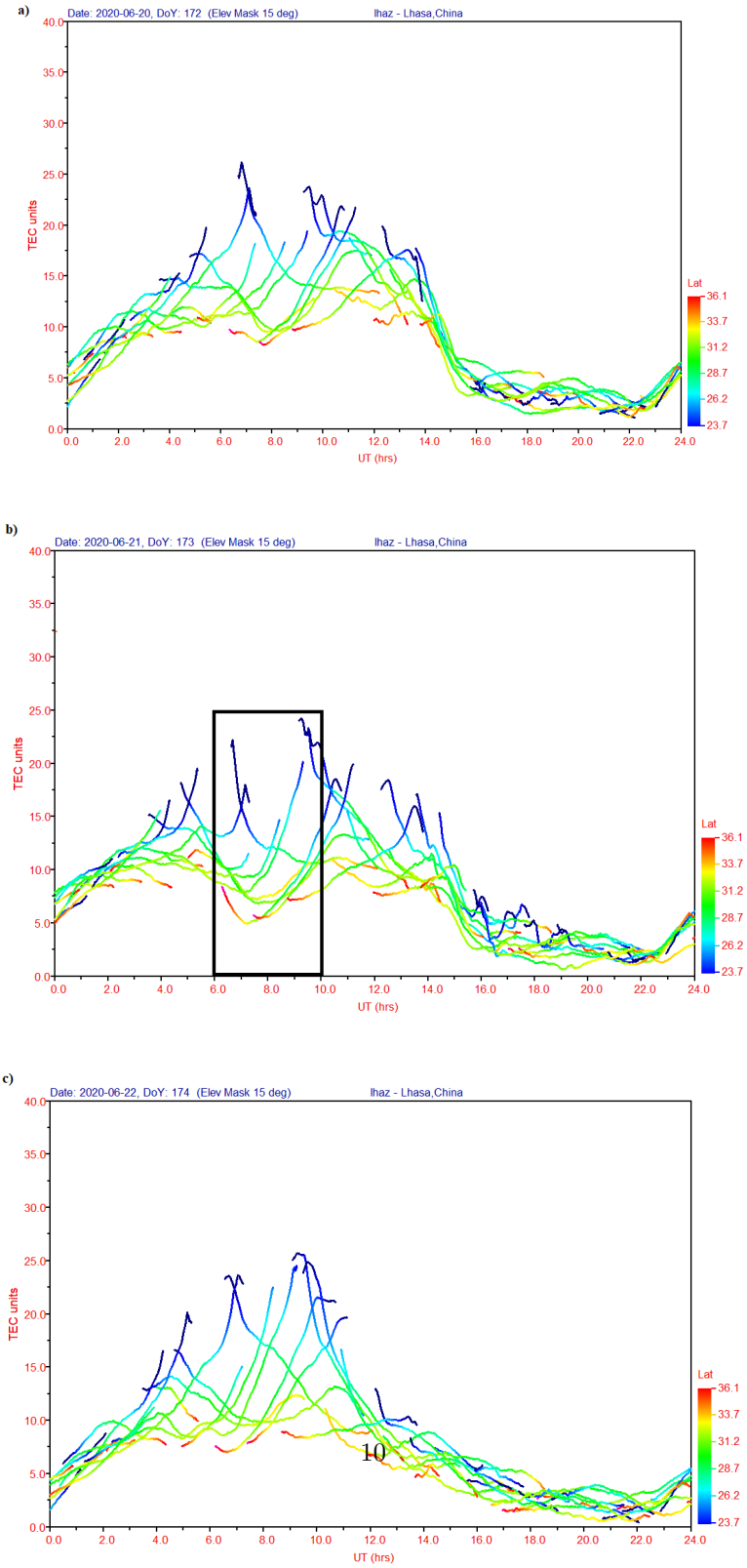

Fig. 5 Daily variation of slant TEC at LHAZ GPS station on (a) 20th, (b) 21st, and (c) 22nd June 2020. The square shows the maximum phase of the solar eclipse at the LHAZ GPS station in China. (The eclipse hours period has been indicated with the black box in column (b)).

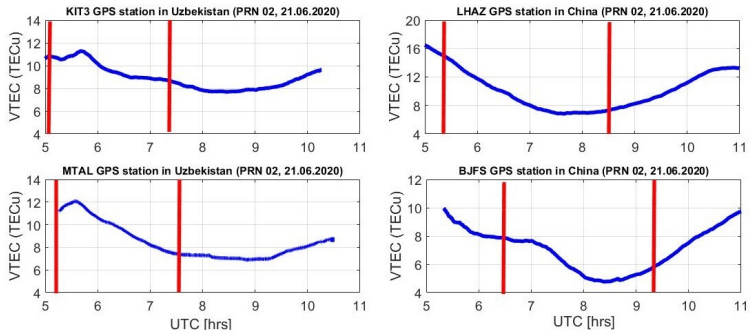

Fig. 6 Variation of vertical TEC for KIT3, MTAL, LHAZ, and BJFS GPS stations during the solar eclipse of 21st June 2020. (The vertical red line highlights the eclipse hours).

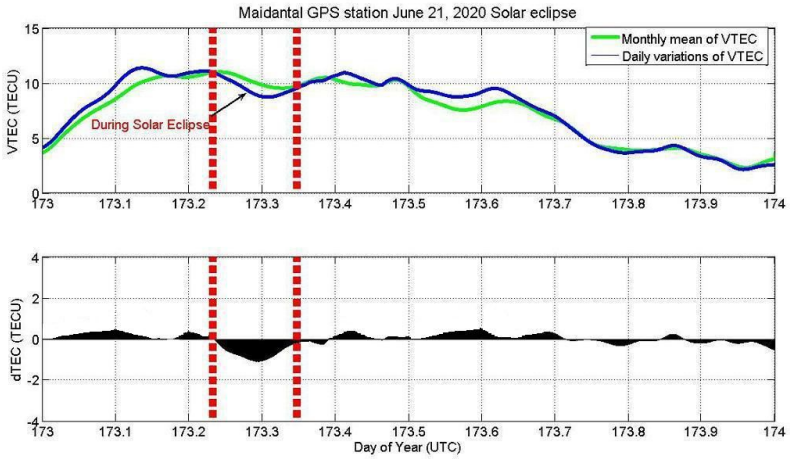

Fig. 7 The decrease of vertical and differential TEC during the Solar eclipse occurred on 21 June 2020 at the MTAL GPS station in Uzbekistan. Vertical dashed lines indicate the start and end of the eclipse.

are presented in Fig. 12. LHAZ GPS station several satellites were observed, i.e. PRN 02, PRN 06, PRN 12, and PRN 25 are presented in Fig. 13. BJFS GPS station several satellites were observed, i.e. PRN 02, PRN 04, PRN 06, and PRN 25 are presented in Fig. 14. Variations of TEC and S4 indices were in observed several satellites at the MTAL GPS station during the annular Solar eclipse, i.e., PRN 02 and PRN 06 are presented in Fig. 19 and MADK GSP station during the annular Solar eclipse, i.e., PRN 02 and PRN 06 are presented in Figure 20

4 Discussion

The ionosphere and the ionospheric formation theory developed in the literature play an important role in the modern ionospheric study. The ionospheric steady state

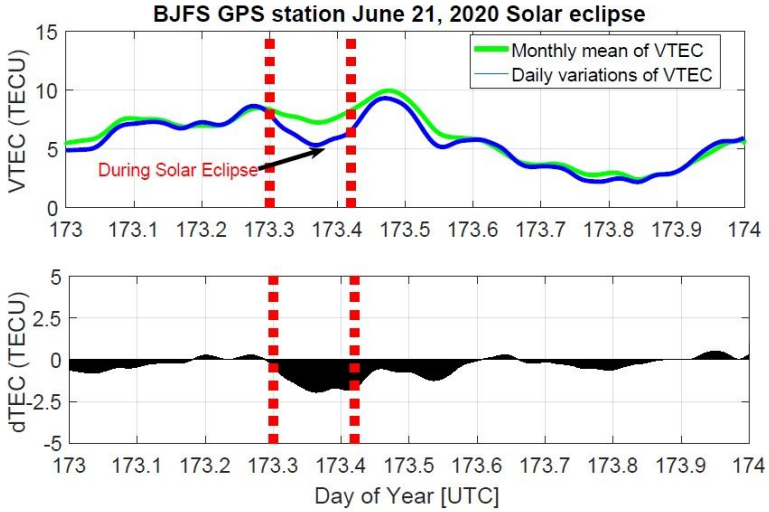

Fig. 8 The decrease of vertical and differential TEC during the Solar eclipse occurred on 21 June 2020 at the BJFS GPS station in China. Vertical dashed lines indicate the start and end of the eclipse.

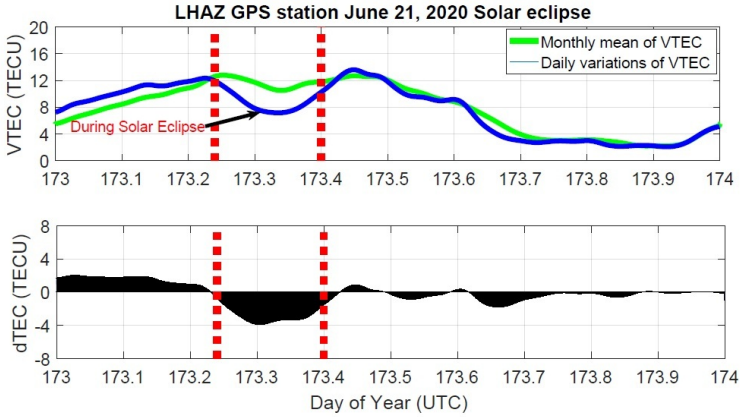

Fig. 9 The decrease of vertical and differential TEC during the Solar eclipse occurred on 21 June 2020 at the LHAZ GPS station in China. Vertical dashed lines indicate the start and end of the eclipse.

is formed on the combined action of the light chemistry, thermodynamics, kinetics, electrodynamics, and other processes [53], [54]. It has not only a complex spatial distribution structure but also has the time-varying characteristics with different time scales which are controlled by multiple mechanisms. In the beginning pioneering stage of active studies of the ionosphere, an observed ionospheric phenomenon that could

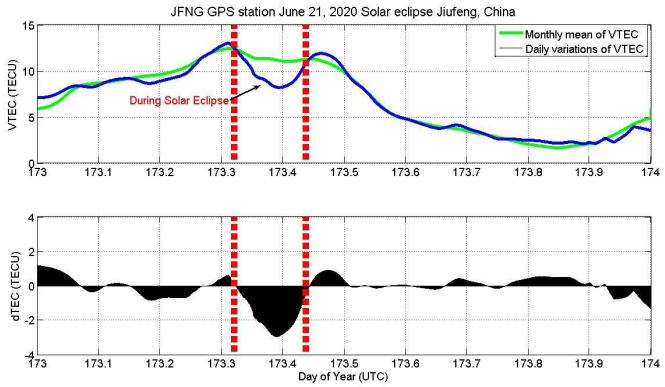

Fig. 10 A decrease of vertical and differential TEC during the Solar eclipse occurred on 21 June 2020 at the JFNG GPS station in China. Vertical dashed lines indicate the start and end of the eclipse.

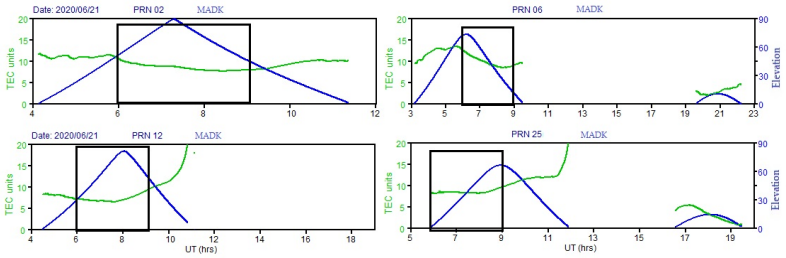

Fig. 11 Variation of TEC with elevation angels along satellite passes PRN 02, PRN 06, PRN 12, and PRN 25 rows for MADK GPS station during the solar eclipse of 21st June 2020. (The black box highlights the from 06:00 until after 09:00 UT hours.

not be explained by the Chapman theory of solar photoionization of the neutral atmosphere [55] was often called anomalous.

Later it was realized that at altitudes (heights of F region) where these anomalies were observed, the plasma was no longer in photochemical equilibrium and that transport processes due to diffusion, neutral winds, and electromagnetic drifts played an important role [56], [57], and deviations from the simple Chapman theory could be expected. The F region is usually divided into three subregions. The lowest region, where photochemistry dominates, is called the F1 region. The region where there is a transition from chemical to diffusion dominance is called the F2 region, and the upper F region, where diffusion dominates, is called the topside ionosphere. In the F1 region, the photochemistry is simplified because only one ion (O^+) dominates. The important reactions are photoionization of neutral atomic oxygen and loss in reactions with N_2 and O_2.

The Figures 7, 8, 9 and 10 show the vertical and differential TEC variations in 21 June 2020 above MTAL, BJFS, LHAZ and JFNG stations, respectively. Vertical red lines denote the duration of the Solar eclipse i.e. beginning and end. Differential TEC is obtained by subtracting monthly averaged diurnal vertical TEC from the values of

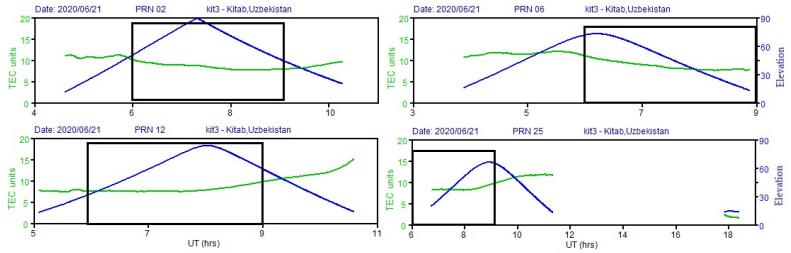

Fig. 12 Variation of TEC with elevation angels along satellite passes PRN 02, PRN 06, PRN 12, and PRN 25 rows for KIT3 GPS station during the solar eclipse of 21st June 2020. (The black box highlights the from 06:00 until after 09:00 UT hours).

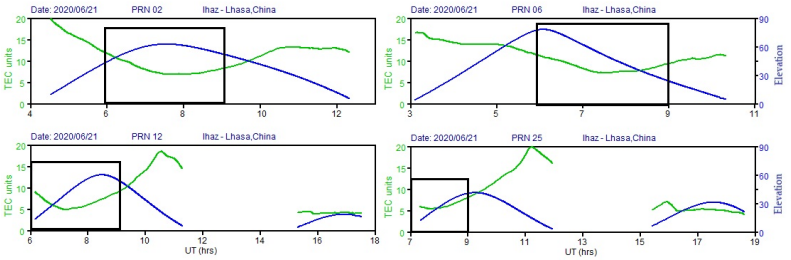

Fig. 13 Variation of TEC with elevation angels along satellite passes PRN 02, PRN 06, PRN 12, and PRN 25 rows for LHAZ GPS station during the solar eclipse of 21st June 2020. (The black box highlights the from 06:00 until after 09:00 UT hours).

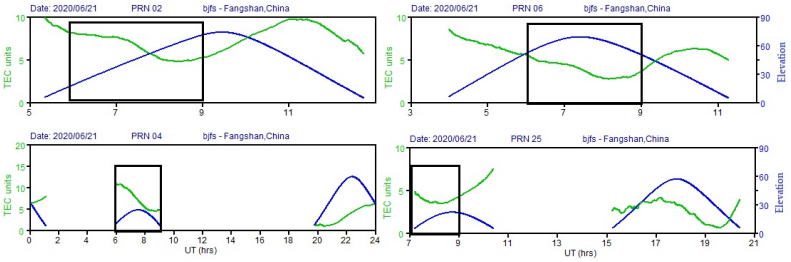

Fig. 14 Variation of TEC with elevation angels along satellite passes PRN 02, PRN 04, PRN 06, and PRN 25 rows for BJFS GPS station during the solar eclipse of 21st June 2020. (The black box highlights the from 06:00 until after 09:00 UT hours).

Table 2 Ionospheric Scintillation Index S4 measurements for GPS stations during continuous three days

GPS stations (2 hours)	S4aver	S4std	S4medi	S4min	S4max	Eclipse Mag (Area)
MTAL (June 20, 2020)	0.0880	0.0957	0.0620	0.0190	0.7830	
MTAL (June 21, 2020)	0.0858	0.0890	0.0570	0.0240	0.7160	0.6119 (52%)
MTAL (June 22, 2020)	0.0965	0.0902	0.0820	0.0170	0.4610	
BJFS (June 20, 2020)	0.0738	0.0289	0.0690	0.0260	0.1980	
BJFS (June 21, 2020)	0.0646	0.0123	0.0680	0.0190	0.2150	0.9663 (95 %)
BJFS (June 22, 2020)	0.0753	0.0381	0.0670	0.0150	0.3250	

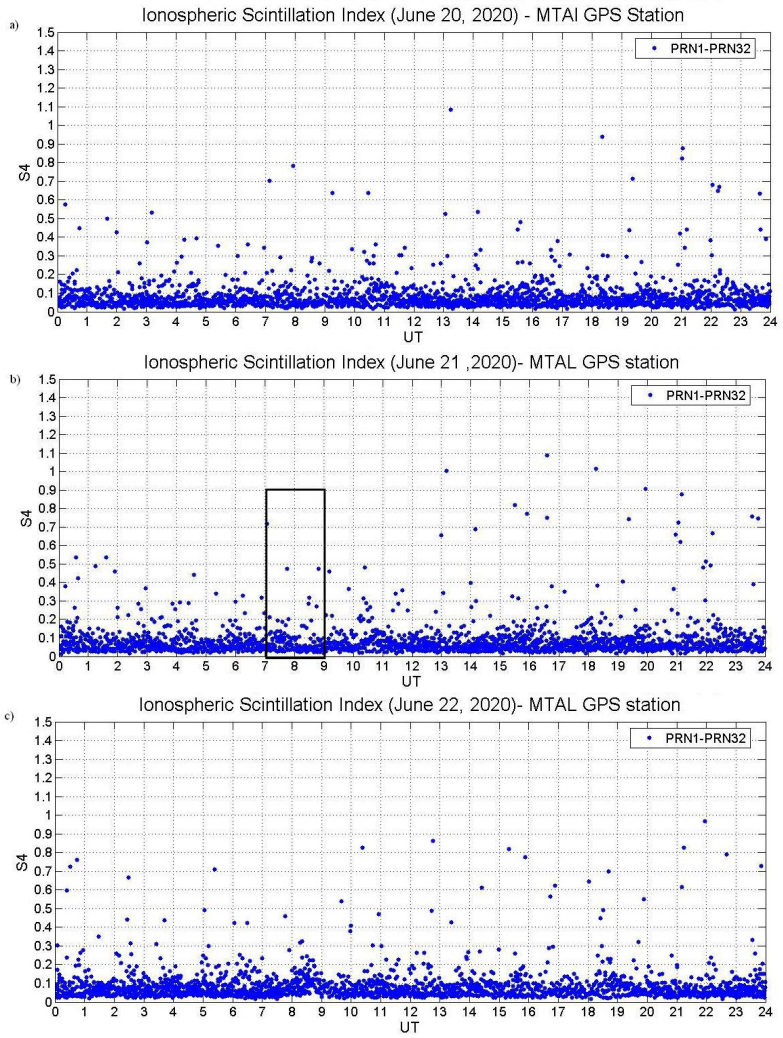

Fig. 15 Diurnal variation of the amplitude scintillation index S_4 values based on data of MTAL station at (a) one day before the eclipse (b) the day of solar eclipse occurrence and (c) one day after the event. (The eclipse hours period has been indicated with the black box).

observed vertical TEC at each epoch. Vertical and Differential TEC variations indicate that differential TEC is decreased during the solar eclipse.

As it can be seen from Figures 15 and 17, Ionospheric Scintillation Index S4 values show a slight reduction during the occurrence of the total solar eclipse, i.e. on the 21st of June from around 07:00 until after 09:00 UT at the stations MTAL (Figure 16.) and BJFS (Figure 18).

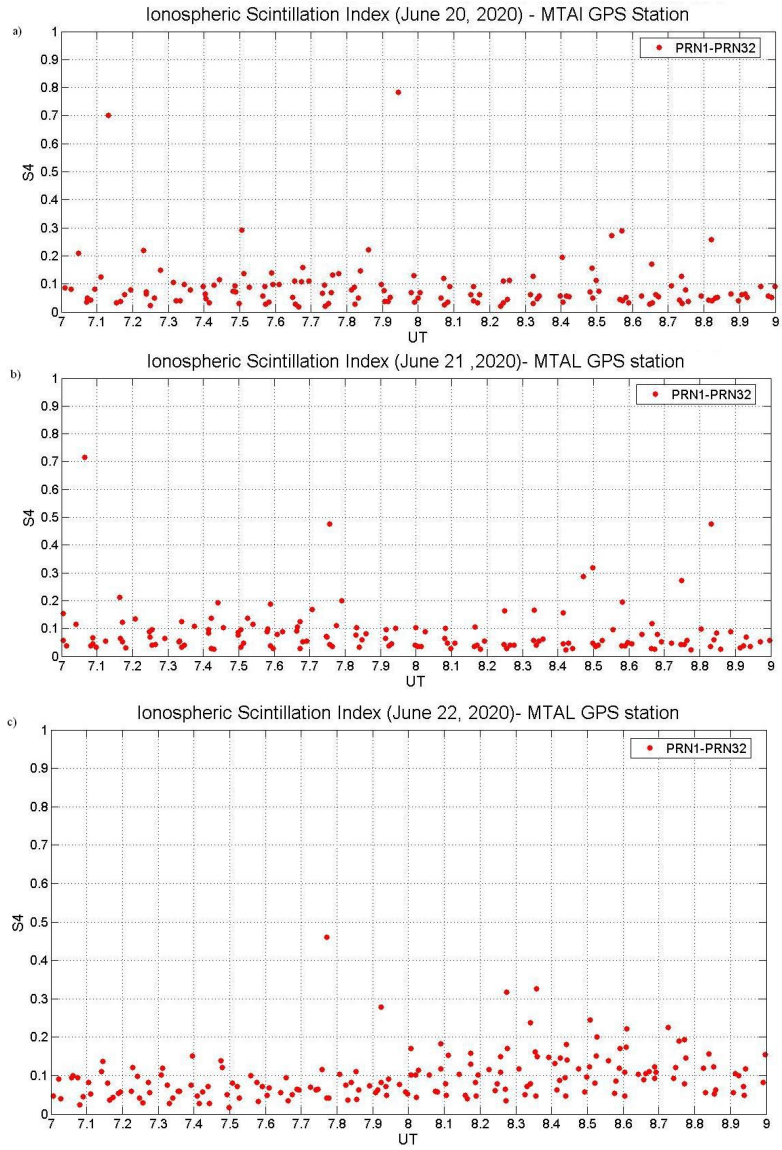

Fig. 16 Variation of the amplitude scintillation index S_4 values based on data of MTAl station during continuous two hours.

5 Conclusions

On June 21st, 2020 an annular solar eclipse was visible in Central and South-East Asia, which offered a great opportunity to study ionospheric behavior under eclipse conditions. In this study, GPS observations over Uzbekistan and China on the day of the eclipse, one day before and one day after its occurrence have been processed to investigate the ionospheric response to this event. Variation in the S_4 values, which

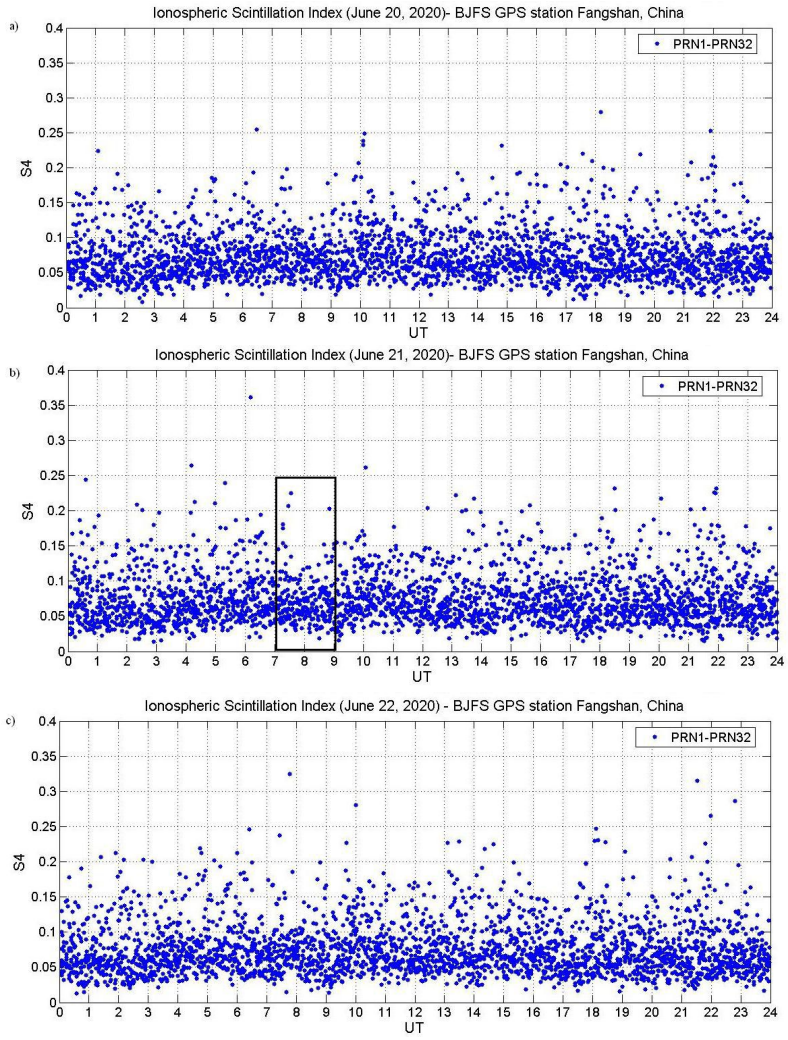

Fig. 17 Diurnal variation of the amplitude scintillation index S_4 values based on data of BJFS station at (a) one day before the eclipse (b) the day of solar eclipse occurrence and (c) one day after the event. (The eclipse hours period has been indicated in the black box).

indicates the variation in the occurrence of ionospheric scintillation, has been studied during the occurrence of a solar eclipse (see Table 2). Although the first two parameters were thoroughly investigated by several authors, studying ionospheric scintillation due to solar eclipse has been investigated for the first time using available stations in Central and South-East Asia. Regarding TEC values, the results at different stations and for each signal path from a satellite to a receiver have shown a reduction between 1 and 5 TECU during the occurrence of the total solar eclipse, which confirms previous studies and also theoretical assumptions ([58], [59]).

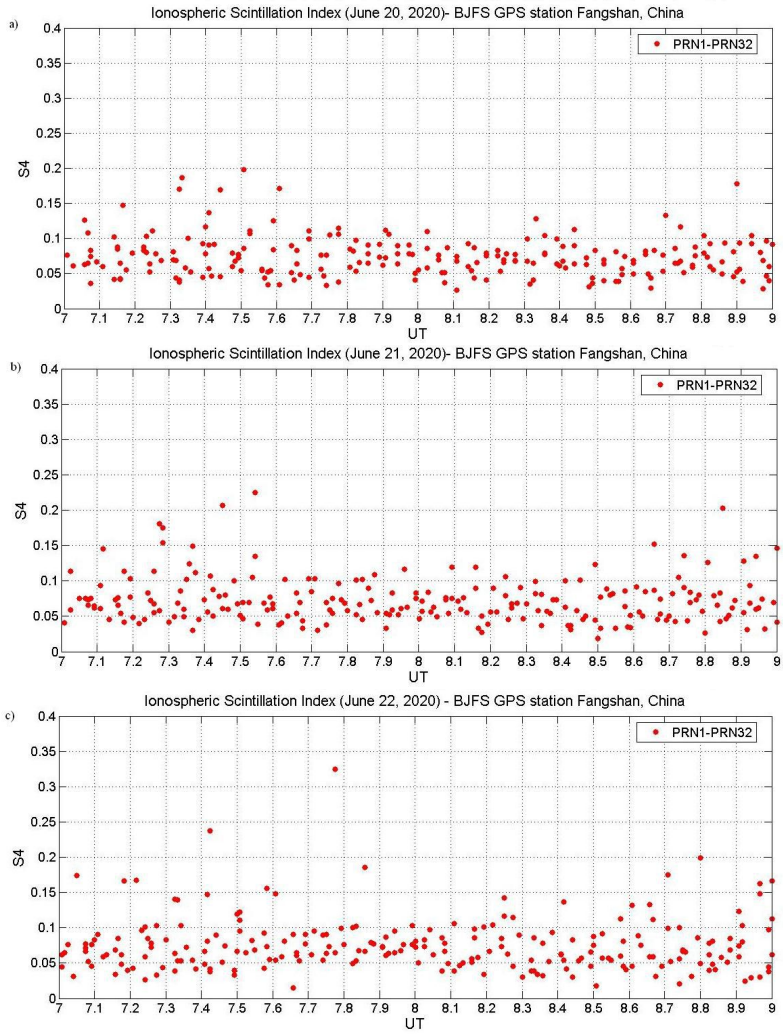

Fig. 18 Variation of the amplitude scintillation index S_4 values based on data of BJFS station during continuous two hours.

Comparing the amplitude scintillation index S_4 values of data based on station MTAL during the annular solar eclipse hours (values within the black box in Fig. 15(b)) with similar time on a day before and a day after the annular solar eclipse has shown a reduction of around 6.94% in the amplitude scintillation index S_4 values. A similar comparison is performed by analyzing data of station BJFS (values within the black box in Fig. 17(b)) which has shown a reduction of 13.34% in the amplitude scintillation index S_4 values. Since the amplitude scintillation index S_4 values are directly related to the occurrence of ionospheric scintillation, it can be concluded that the ionospheric scintillation has been valuably reduced in two GPS stations during the occurrence of the annular solar eclipse.

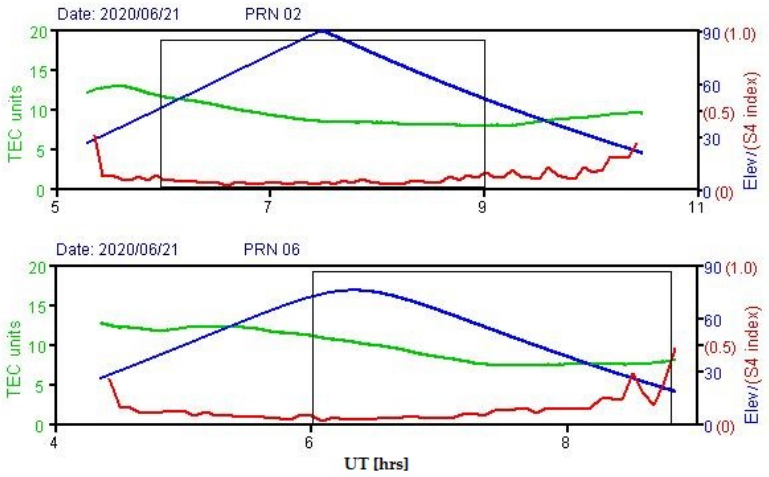

Fig. 19 Variations of TEC and S4 indices along satellite passes (PRN 02 and PRN 06 rows, respectively) for MTAL GPS station during the solar eclipse of 21st June 2020. (The black box highlights the from 06:00 until after 09:00 UT hours).

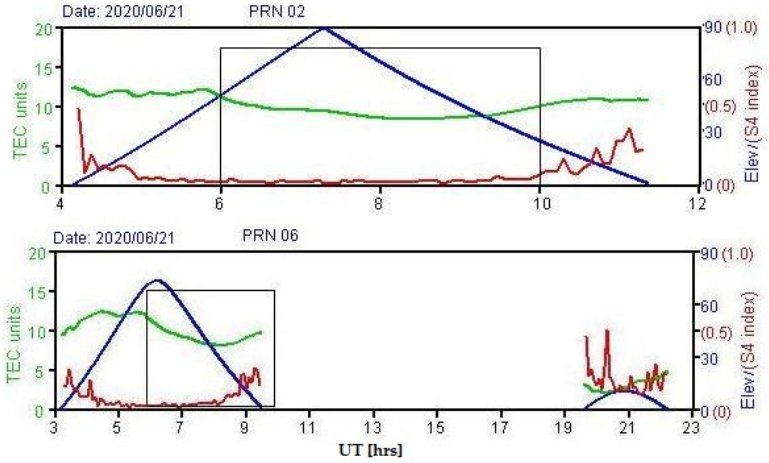

Fig. 20 Variations of TEC and S4 indices along satellite passes (PRN 02 and PRN 06 rows, respectively) for MADK GPS station during the solar eclipse of 21st June 2020. (The black box highlights the from 06:00 until after 10:00 UT hours).

References

[1] Shrivastava, M.N., Maurya, A.K. and Kumar, K.N. Ionospheric perturbation during the South American total solar eclipse on 14th December 2020 revealed with the Chilean GPS eyeball. Sci Rep 11, 20324. https://doi.org/10.1038/s41598-021-98727-w, (2021).

[2] Maurya, A. K. et al. Low-mid latitude D region ionospheric perturbations associated with 22 July 2009 total solar eclipse: Wave-like signatures inferred from VLF observations. J. Geophys. Res. Space Physics 119 (10), 8512–8523 (2014).

[3] Chimonas, G. Internal gravity-wave motions induced in the Earth's atmosphere by a solar eclipse. J. Geophys. Res. 75(28), 5545–5551 (1970).

[4] Antonia, R. A., Chambers, A. J., Phong-Anant, D., Rajagopalan, S. and Sreenivasan, K. R. Response of atmospheric surface layer turbulence to a partial solar eclipse. J. Geophys. Res. 84(C4), 1689–1692 (1979).

[5] Cohen E.A., The study of the effect of solar eclipse on the ionosphere based on satellite beacon observation, Radio Sci., 19, 3, 769-777, (1984).

[6] Salah J.E., Oliver W.L., Foster J.C., and Holt J.M., Observation of the May 30, 1984, Annular Solar Eclipse at Millstone Hill, J. Geophysical Research, 91, A2, 1651-1660 (1986).

[7] Yeh K.C., Yu D.C., Lin K.H., Liu C.H., Huang C.R. et al., Ionospheric response to a solar eclipse in the equatorial anomaly region, Terr.Atmos. and Oceanic Science, 8,2, 165-178 (1992).

[8] Clilverd MA, Rodger CJ, Thomson NR. Total solar eclipse effects on VLF signals: Observations and modeling. Radio Sci. 36:773.(2001).

[9] Chakrabarti SK, Mondal SK, Sasmal S. VLF signals in summer and winter in the Indian sub-continent using multi-station campaigns. Indian J Phys. 86:323–334.(2012).

[10] Inan US, Lehtinen NG, Moore RC, Hurley K, Boggs S, Smith DM, Fishman GJ. Massive disturbance of the daytime lower ionosphere by the giant g-ray flare from magnetar SGR 1806-20. Geophys. Res. Lett. 34:L08103.(2007).

[11] Yuan, T.; Wang, J.; Cai, X.; Sojka, J.; Rice, D.; Oberheide, J.; Criddle, N. Investigation of the seasonal and local time variations of the high-altitude sporadic Na layer (Nas) formation and the associated midlatitude descending E layer (Es) in lower E region. J. Geophys. Res. Space Phys. 2014, 119, 5985–5999.

[12] Schunk, R. W., Nagy, A. F. Ionospheres: Physics, Plasma Physics, and Chemistry (2nd ed.). Cambridge, UK: Cambridge University Press. https://doi.org/10.1017/CBO9780511635342.(2009).

[13] Tian, Z., Sui, Y., Zhu, S., and Sun, Y.Y. (2022). Enhancement of electron density in the ionospheric F2 layer near the first contact of the total solar eclipse on 21 August 2017. Earth and Space Science, 9, e2021EA002016. https://doi.org/10.1029/2021EA002016, (2021).

[14] Ding, F., et al.: GPS TEC response to the 22 July 2009 total solar eclipse in East Asia, J. Geophys. Res., 115, A07308, doi:10.1029/2009JA015113, (2010).

[15] Sharma, S., Dashora, N., Galav, P., and Pandey, R.: Total solar eclipse of July 22, 2009: Its impact on the total electron content and ionospheric electron density in the Indian zone, J. Atmos. Solar-Terr. Phys., 72, 1387–1392, (2010).

[16] Galav, P., Sharma, S., and Pandey, R.: Study of simultaneous penetration of electric fields and variation of total electron content in the day and night sectors during the geomagnetic storm of 23 May 2002, J. Geophys. Res., 116, A12324, doi:10.1029/2011JA017002, (2011).

[17] Kumar, S., and Singh, A. K.: Changes in Total Electron Content (TEC) during the Annular Solar Eclipse of 15 January 2010, Adv. Space. Res., 49, 75–82, (2012).

[18] Jayakrishnan, P. R., Babu, C.A., and Sivaprasad, P.: Drastic Variation in surface boundary layer parameters over Cochin, during the annular solar eclipse: analysis using anemometer data, J.atmos. Solar-Terr. Phys., 94, 49-53, 10.1016/j.jastp.2012.12.019, (2013).

[19] Farges, T., Pichon, A Le Blanc, E., Perez,S., and Alcoverro, B.: Response of the lower atmosphere and ionosphere to the eclipse of August 11,1999, J. Atmos. Solar-Terr. Phys., 65,717-726, doi:10.1016/S1364-6826(03)00078-6, (2003).

[20] Şentürk, E., Arqim Adil, M., and Saqib, M. (2021). Ionospheric total electron content response to annular solar eclipse on June 21, 2020. Advances in Space Research, 67(6), 1937-1947. https://doi.org/10.1016/j.asr.2020.12.024.

[21] Huang, F., Li, Q., Shen, X., Xiong, C., Yan, R., Zhang, S., Wang, W., Aa, E., Zhong, J., Dang, T., and Lei, J. (2020). Ionospheric Responses at Low Latitudes to the Annular Solar Eclipse on 21 June 2020. Journal of Geophysical Research: Space Physics, 125(10). https://doi.org/10.1029/2020ja028483.

[22] Aa, E., Zhang, S.-R., Shen, H., Liu, S., and Li, J. (2021). Local and conjugate ionospheric total electron content variation during the 21 June 2020 solar eclipse. Advances in Space Research, 68(8), 3435-3454. https://doi.org/10.1016/j.asr.2021.06.015.

[23] Wang, J., Sun, Y., Yu, T., Wang, Y., Mao, T., Yang, H., Xia, C., Yan, X., Yang, N., Huang, G., and Yifan qi. (2022). Convergence Effects on the Ionosphere During and After the Annular Solar Eclipse on 21 June 2020. Journal of Geophysical Research: Space Physics, 127(9). https://doi.org/10.1029/2022ja030471.

[24] Dang, T., Lei, J. H., Wang, W. B., Yan, M. D., Ren, D. X., and Huang, F. Q. (2020). Prediction of the thermospheric and ionospheric responses to the 21 June 2020 annular solar eclipse. Earth Planet. Phys., 4(3), 231–237. http://doi.org/10.26464/epp2020032.

[25] Qiao, L.; Chen, G.; Gong, W.; Cai, X.; Liu, E.; Su, M.; Teng, X.; Qiu, Z.; Song, H. E-Region Field- Aligned Irregularities in the Middle of a Solar Eclipse Observed by a Bistatic Radar. Remote Sens., 14, 392. https://doi.org/10.3390/rs14020392.(2022).

[26] Baran,L., Ephishov,I., Shagimuratov,I., Ivanov,V., Lagovsky,A. The response of the ionospheric total electron content to the solar eclipse on August 11, 1999, Adv. Space Res. 31 (4), 989-994 (2003).

[27] J. Ratcliffe, A survey of solar eclipses and the ionosphere. Solar Eclipses and the Ionosphere, J. Atmos. Terr. Phys. 6 (Special suppl) 1-13,(1956).

[28] H. Rishbeth, Solar eclipses and ionospheric theory, Space Sci. Rev. 8 (4), 543-554, (1968).

[29] Afraimovich E., Palamartchouk K., Perevalova N., Chernukhov V., Lukhnev A., Zalutsky V. Ionospheric effects of the solar eclipse of March 9, 1997, as deduced from GPS data, Geophys. Res. Lett. 25 (4) 465-468 (1998).

[30] J.A. Klobuchar, H. Whitney, Ionospheric electron content measurements during a solar eclipse, J. Geophys. Res. 70 (5) 1254-1257 (1965).

[31] S. Kumar, A. Singh, R. Singh, Ionospheric response to total solar eclipse of 22 July 2009 in different Indian regions, Ann. Geophys. 31, 1549-1558,(2013).

[32] T. Farges, J. Jodogne, R. Bamford, Y. Le Roux, F. Gauthier, P. Vila, D. Altadill, J. Sole, G. Miro, Disturbances of the western European ionosphere during the total solar eclipse of 11 August 1999 measured by a wide ionosonde and radar network, J. Atmos. Sol. Terr. Phys. 63 (9), 915-924 (2001).

[33] A.J. Coster, L. Goncharenko, S.R. Zhang, P.J. Erickson, W. Rideout, J. Vierinen. GNSS observations of ionospheric variations during the 21 August 2017 solar eclipse, Geophys. Res. Lett. 44 (24),12,041-112,048 (2017).

[34] I. Cherniak, I. Zakharenkova, Ionospheric total electron content response to the great American solar eclipse of 21 August 2017, Geophys. Res. Lett. 45 (3) 1199-1208 (2018).

[35] Salah J.E., Oliver W.L., Foster J.C., and Holt J.M., Observation of the May 30, 1984, Annular Solar Eclipse at Millstone Hill, J. Geophysical Research, 91, A2, 1651-1660 (1986).

[36] Briggs B.H, Parkin I.A. On the variation of radio star and satellite scintillations with zenith angle. J. Atmos. Terr. Phys. 25(6), 339-366 (1963).

[37] Tillayev, Y.; Azimov, A.; Hafizov, A. Astronomical Seeing at Maidanak Observatory during the Year 2018. Galaxies 2021, 9, 38.

https://doi.org/10.3390/galaxies9020038 (2021).

[38] Shikhovtsev, A.Y.; Kovadlo, P.G.; Kopylov, E.A.; Ibrahimov, M.A.; Ehgamberdiev, S.A.; Tillayev, Y.A. Energy Spectra of Atmospheric Turbulence for Calculating C2n Parameter. I. Maidanak and Suffa Observatories in Uzbekistan. Atmosphere 2021, 12, 1614. https://doi.org/10.3390/atmos12121614, (2021).

[39] Tojiev, S.R., Ahmedov, B.J., Tillayev, Y.A., Eshkuvatov, H.E. Ionospheric anomalies of local earthquakes detected by GPS TEC measurements using data from Tashkent and Kitab stations. Advances in Space Research 52,1146-1154 (2013).

[40] Tojiev, S.R., Ahmedov, B.J., Eshkuvatov, H.E. Ionospheric precursors of earthquakes recorded by VLF receiver at Tashkent IHY station. Advances in Space Research 54, 628-643(2014).

[41] Tojiev, S.R., Morozova, V.S., Ahmedov, B.J. and Eshkuvatov, H.E. Electromagnetic Studies of Ionospheric and Magnetospheric Perturbations Associated with The Earth, Atmospheric and Astrophysical Phenomena, Mathematical Physics, World Scientific, pp.254-278 (2012).

[42] H.E. Eshkuvatov, B.J. Ahmedov, Y.A. Tillayev, M.Arslan Tariq, Libo Liu, M. Ali Shah. Ionospheric precursors of strong earthquakes observed using six GNSS stations data during continuous five years (2011-15). Geodesy and Geodynamics Volume 14, Issue 1, January 2023, Pages 65-79.

[43] Theodore, L. B., Paul, M.K. Simultaneous Global Positioning System observations of equatorial scintillations and Total Electron Content fluctuations. Journal of Geophysical Research, 104 (A10), 22553-22565 (1999).

[44] Seemala, G. K., and C. E. Valladares (2011), Statistics of total electron content depletions observed over the Southern American continent for the year 2008, Radio Sci., 46, RS5019, doi:10.1029/2011RS004722.

[45] Klobuchar, J.A.: Design and characteristics of the GPS ionospheric time delay algorithm for single frequency users. In: Institute of Electrical and Electronics Engineers, pp. 280–286, (1986).

[46] Ahmedov B.J, Tojiev S.R., Eshkuvatov H.E. Total Electron Content (TEC) Extraction using Kitab and Tashkent GPS stations, Uzbek Journal of Physics, 6, pp361-366 (2016).

[47] Ahmedov B.J, Tojiev S.R., Eshkuvatov H.E. Low radiofrequency radiation in the D-layer of the ionosphere and possibility of their registration on Tashkent VLF station , Uzbek Journal of Physics, Vol.17, 6, pp.339-350, (2015) .

[48] Yeh K.C, Liu C-H (1982) Radio wave scintillations in the ionosphere. IEEE Proceedings 70:324–360. https://doi.org/10.1109/proc.1982.12313.

[49] Aol, S., Buchert, S. and Jurua, E. Ionospheric irregularities and scintillations: a direct comparison of in situ density observations with ground-based L-band receivers. Earth Planets Space 72, 164 (2020). https://doi.org/10.1186/s40623-020-01294-z.

[50] Streets RBJ .Variation of radio star and satellite scintillations with sunspot number and geomagnetic latitude. J Can Soc Expl Geophys 5:35-52, (1969).

[51] Fremouw, E.J., Leadabrand, R.L., Livingstone, R.C., Cousin, M.D., Rino, C.L., Fair, B.C., Long, R.A. Early results from the DNA Wideband satellite experiment - complex signal analysis. Radio Sci. 13 (1), 167-187 (1978).

[52] Cai, X., Burns, A. G., Wang, W., Qian, L., Pedatella, N., Coster, A., et al. (2021). Variations in thermosphere composition and ionosphere total electron content under "geomagnetically quiet" conditions at solar-minimum. Geophysical Research Letters, 48, e2021GL093300. https://doi.org/10.1029/2021GL093300.

[53] Xiong, C., Lühr, H., and Yamazaki, Y. (2019). An opposite response of the low-latitude ionosphere at Asian and American sectors during storm recovery phases: Drivers from below or above. Journal of Geophysical Research: Space Physics, 124, 6266–6280. https://doi.org/10.1029/2019JA026917.

[54] Wan, X., Xiong, C., Gao, S. et al. The nighttime ionospheric response and occurrence of equatorial plasma irregularities during geomagnetic storms: a case study. Satell Navig 2, 23 (2021). https://doi.org/10.1186/s43020-021-00055-x.

[55] Chapman, S. (1931), The absorption and dissociative or ionizing effect of monochromatic radiation in an atmosphere on a rotating Earth, Proc. Phys. Soc., 43, 26-45.

[56] Hanson, W. B., and R. J. Moffett (1966), Ionization transport effects in the equatorial F region, J. Geophys. Res., 71 (23), 5559-5572, doi:10.1029/JZ071i023p05559.

[57] Rishbeth, H. (1967), The effect of winds on the ionospheric F2-peak, J. Atmos. Terr. Phys., 29, 225-238.

[58] Y. Jiao, Y. Morton, S. Taylor, Comparative studies of high-latitude and equatorial ionospheric scintillation characteristics of GPS signals, in: 2014 IEEE/ION Position, Location and Navigation Symposium-PLANS, pp. 37-42 (2014).

[59] Mohamad Mohdi Alizadeh, Harald Schuh, Saeed Zare, Sahar Sobhkhiz-Miandehi, lung-Chin Tsai. Remote sensing ionospheric variations due to total solar eclipse, using GNSS observations, Geodesy and Geodynamics 11, 202-210 (2020).